RSC Advances

PAPER

View Article Online
View Journal | View Issue

Check for updates

Cite this: *RSC Adv.*, 2025, **15**, 38201

Properties of human centrin 2 and cooperative effects between the N- and C-terminal domains

Jing Yang, [a] Yaqin Zhao [b] and Binsheng Yang *[b]

Human centrin 2 (HsCen2) is a Ca^{2+}-binding protein belonging to the highly conserved calmodulin superfamily, and it is organized by two domains, namely, N-terminal and C-terminal domains. However, the combined effect between the N- and C-terminal domains of HsCen2 is not clear. The aggregation and the endonuclease-like activities of HsCen2 and their isolated C-terminal and N-terminal domains (C-HsCen2 and N-HsCen2) were investigated by isothermal titration calorimetry (ITC), far-UV CD spectroscopy, DOCK analysis, and agarose gel electrophoresis in 10 mM Hepes, pH 7.4. The results proved the presence of a cooperative effect between the N- and C-terminal domains of HsCen2. The presence of the N-terminal domain facilitated the binding of Tb^{3+} to the C-terminal domain of HsCen2 and enhanced Tb^{3+}-induced HsCen2 aggregation. Interestingly, DNA can bind to HsCen2 or C-HsCen2 or N-HsCen2, and the affinity of C-HsCen2 binding to DNA is stronger than that of intact HsCen2 to DNA. In addition, HsCen2, isolated C-HsCen2, and isolated N-HsCen2 exhibited endonuclease-like activities that induced DNA strand break through the hydrolysis pathway, and the endonuclease-like activity was of the following order: N-HsCen2 > C-HsCen2 > HsCen2. The results are extensively discussed, and the cooperative effect between the N- and C-terminal domains of HsCen2 is explored.

Received 14th June 2025
Accepted 23rd September 2025

DOI: 10.1039/d5ra04219d

rsc.li/rsc-advances

Open Access Article. Published on 14 October 2025. Downloaded on 6/14/2026 6:45:11 PM.
This article is licensed under a Creative Commons Attribution-NonCommercial 3.0 Unported Licence.

1. Introduction

Similarly to calmodulin, centrin consists of two globular lobes: N-terminal and C-terminal domains, connected by a flexible linker.[1] It contains four helix-loop-helix topology structures, known as the EF-hand subdomain.[2,3] Centrins have four EF-hand domains, but their ability to bind Ca^{2+} varies widely.[4] For example, Human centrin 1 (HsCen1) has four Ca^{2+}-binding sites, two high-affinity sites at the C-terminal, and two low-affinity sites at the N-terminal.[5,6] Human centrin 2 (HsCen2) has two functional Ca^{2+} binding sites in EF-3 and EF-4.[3,7] Human centrin 3 (HsCen3) has one Ca^{2+}/Mg^{2+} mixed binding site with high affinity and two Ca^{2+}-specific sites with low affinity.[8,9] The selective binding of Ca^{2+} to centrin *via* EF-hands may result in α-helix rearrangement and change in conformation from a "closed" to an "open" state.[6,10] After binding Ca^{2+}, the exposed hydrophobic surfaces of protein can interact with other proteins involved in cell signal transduction.[11]

Metal ions play an important role in the life system by helping to maintain the advanced structure of the protein. Metal ions combine with appropriate proteins to form metalloproteins that drive different biological functions in the body.[12] Studies have shown that metal ions can induce the aggregation of centrins.[13,14] Previous research in our lab shows that the N-terminal domain plays a key role in the self-assembly process of *Euplotes octocarinatus* centrin (EoCen).[12,15] Although highly sequence identical with calmodulin (50%), the centrin has a number of different properties such as self-assembly based on the disorder region of the first 20 amino acids.[7,16]

HsCen2 is a typical Ca^{2+}-binding protein, belonging to the highly conserved calmodulin superfamily.[13] It has 172 amino acid residues and contains four EF-hand domains. However, there are only two EF-hand domains localized at the C-terminal domain to bind the metal ion (Fig. 1). HsCen2 was first

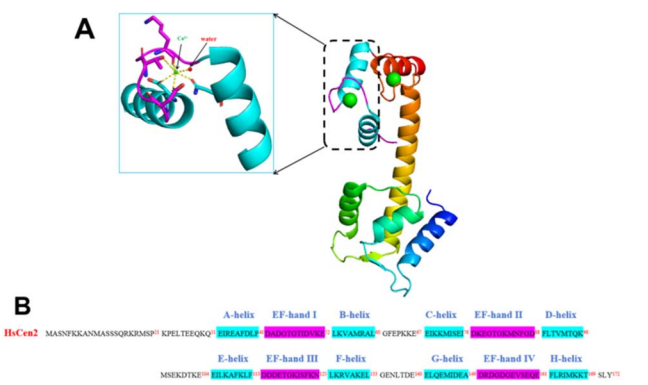

Fig. 1 (A) Structure and EF-hand Ca^{2+}-binding domains of HsCen2 (PDB:2GGM). Ca^{2+}: green; H_2O: red. (B) Protein sequence of HsCen2. The central 12 residues in the EF-hand domains (purple) and α-helices (blue) are highlighted.

[a]*Department of Materials and Chemical Engineering, Taiyuan University, Taiyuan, 030032, China*

[b]*Institute of Molecular Science, Key Laboratory of Chemical Biology of Molecular, Shanxi University, Taiyuan 030006, China. E-mail: yangbs@sxu.edu.cn; Fax: +86 351 7016358*

© 2025 The Author(s). Published by the Royal Society of Chemistry

Open Access Article. Published on 14 October 2025. Downloaded on 6/14/2026 6:45:11 PM. This article is licensed under a Creative Commons Attribution-NonCommercial 3.0 Unported Licence.

discovered in the distal lumen of centrioles, and is ubiquitously expressed.[17] Its presence is required for normal centriole duplication during the cell cycle.[17] In human cells, centrin 2 protein subpopulations are localized to the centrosomes, and centrin 2 phosphorylation during the G2/M phase is required for centriole separation during centrosome duplication.[18] In addition, the inhibition of centrin 2 expression by RNA interference in human cells fails centriole duplication.[13] It has been reported that most centrin 2 protein subpopulations are unrelated to the centrosome, and that about half of them are found in the nucleus;[19] HsCen2 in the nucleus plays a key role in the nuclear excision repair (NER) process.[20–22] We have proved that HsCen2 can bind DNA directly and that HsCen2 exhibits certain endonuclease-like activity to hydrolyze double-stranded DNA.[23]

To understand the difference between the properties of HsCen2 and half-molecules, we first constructed isolated N-HsCen2 (1–100) and C-HsCen2 (82–172) segments. In this work, HsCen2 interactions with Tb^{3+} or DNA were characterized by fluorescence of Tb^{3+}, isothermal titration calorimetry (ITC), far-UV CD spectroscopy, DOCK, and gel electrophoresis in 10 mM Hepes, pH 7.4. The results showed that the N-terminal domain of HsCen2 is inactive although the isolated N-HsCen2 can bind Tb^{3+} or DNA, while the C-terminal domain of HsCen2 and isolated C-HsCen2 has a different affinity for Tb^{3+} or DNA. In addition, the aggregation function, as well as the endonuclease-like activity of HsCen2 and isolated C-HsCen2 or isolated N-HsCen2, is also different. Such knowledge will shed light on the cooperative effect between the N-terminal and C-terminal domains of HsCen2.

2. Experimental

2.1 Reagents

pBR322 DNA was purchased from Sigma corporation. Calf thymus DNA (CT-DNA) was purchased from Solarbio corporation. 4-(2-Hydroxyethyl)-1-piperazineethanesulfonic acid (Hepes) was purchased from Sangon corporation in Shanghai. Protein kinase A (PKA), a cyclic AMP (cAMP)-dependent serine/threonine kinase, was obtained through self-purification for this study. And PreScission Protease (PPase) from self-purification.[24] Other chemicals were of the highest purity available from local sources.

2.2 Protein preparation

Using a full-length HsCen2 plasmid as the template, specific primers designed and synthesized were used to amplify the N-HsCen2 (1–100) and C-HsCen2 (82–172) target genes by the polymerase chain reaction (PCR) technique. The synthesized target genes were connected to the pGEX-6p-1 vector enzymatically, and the cloning results were confirmed by DNA sequence detection. The recombinant plasmids were expressed, isolated, and purified, as described previously.[10] To remove the contaminating bound cations, the protein was first pre-treated with EDTA forming HsCen2 or C-HsCen2 or N-HsCen2 and then passed through a Sephadex G-25 column equilibrated in Hepes buffer, at pH 7.4. The protein concentration of HsCen2 or C-HsCen2 was measured using a molar extinction coefficient at 280 nm of 1490 M^{-1} cm^{-1}. Since there is no luminescent amino acid tyrosine (Tyr) or tryptophan (Trp) in isolated N-HsCen2, the protein concentration cannot be determined by measuring the absorbance, so the bicinchoninic acid (BCA) protein concentration determination kit was used for determination. The production of proteins was confirmed using 15% SDS-PAGE (Fig. S1).

2.3 Aromatic residue-sensitized Tb^{3+} fluorescence

Tb^{3+}-sensitized fluorescence experiments were carried out in 10 mM Hepes (pH 7.4) buffer at room temperature. The scanning range of the Tb^{3+} emission fluorescence spectrum was 470–650 nm, and the excitation wavelength was set at 295 nm. Both slit widths for excitation and emission were 10 nm. The protein (10 μM) was titrated with Tb^{3+} solution at 1 mM, 5 μL was added each time, and the corresponding emission spectra were recorded after 3 min of reaction.

2.4 Far-UV CD

The interactions of HsCen2, C-HsCen2, and N-HsCen2 with Tb^{3+} or DNA and the guanidine hydrochloride (GdnHCl)-induced unfolding of proteins were measurements using circular dichroism (CD) (Applied Photophysics qCD (France)). CD spectra were recorded from 190 to 320 nm at room temperature using 1 mm quartz cells.

2.5 Isothermal titration calorimetry (ITC)

Thermodynamic parameters of intermolecular interactions were investigated by ITC using a MicroCal iTC200 device (MicroCal, Northampton, MA, USA) at 30 °C. The protein and DNA were dissolved in 10 mM Hepes (pH 7.4) and degassed before their use. An ITC instrument contains two identical cells: one for the sample and another for the reference solution. Titration of DNA (5 mM) to protein (80 μM) *via* automatic injections, a total of 30 drops, each injection of 1 μ, and the interval is 3 min. The integration of the heat peaks corresponding to each injection and correction for the baseline, using the origin-based software, gives the enthalpy variation along the mixing path, which represents the reaction isotherm. By fitting the data into the interaction model, the stoichiometric number (n), equilibrium binding constant (K_a), and interaction enthalpy (ΔH) were obtained.

The method of preparation of CT-DNA was referred from the literature.[25] The DNA solutions used were CT-DNA solutions in all spectroscopic experiments.

2.6 Fluorescence spectroscopy

A HITACHI F-2700 spectrofluorometer (HORIBA Jobin Yvon, France) was used to record the fluorescence spectra of intermolecular interactions. For the binding of HsCen2 or C-HsCen2 (10 μM) with DNA (5 mM), the excitation wavelength was set at 280 nm. Both excitation and emission slit widths were 10 nm. The emission spectra were recorded from 295 to 500 nm. With the increasing DNA concentration, the corresponding emission

 © 2025 The Author(s). Published by the Royal Society of Chemistry

Open Access Article. Published on 14 October 2025. Downloaded on 6/14/2026 6:45:11 PM. This article is licensed under a Creative Commons Attribution-NonCommercial 3.0 Unported Licence.

spectra were recorded. The reported constants are averages of three experiments.

2.7 Molecular docking simulation

The ZDOCK 3.0.2 software was used to simulate intermolecular interactions (http://zdock.umassmed.edu).[26] The structures of DNA duplex (PDB:1DJD), HsCen2, or N-HsCen2 (PDB:2GGM) were obtained from the PDB database. The binding mode of DNA and HsCen2 or N-HsCen2 was simulated by the automatic docking software, and the optimal complex structure was found through a global search.

2.8 Resonance light scattering measurements

The turbidity of the solution was detected using a HITACHI F-2700 spectrophotometer to determine the resonance light scattering (RLS) of the protein sample. The detection signal used synchronous fluorescence from 250 to 600 nm, and the excitation and emission slits were set at 10 nm. The protein (10 μM) was titrated with a Tb^{3+} solution (1 mM), 5 μL was added each time, and the corresponding RLS spectra were recorded after 3 min. The dilution effect of titration was deducted in the data processing. All fluorescence experiments were conducted in 10 mM Hepes at pH 7.4 and room temperature.

2.9 Cleavage of pBR322 DNA

A mixture of 0.005 μg μL^{-1} pBR322 DNA and protein sample was incubated in 10 mM Hepes buffer (pH 7.4) for a certain period to carry out the cleavage reaction of pBR322 DNA. All samples were added to a 1% agarose gel containing 4S Red Plus Nucleic Acid Stain. Electrophoresis was carried out at a constant voltage of 130 eV in 1×TAE (tris-acetic-EDTA), and the electrophoresis time was about 30 min. DNA reaction products were analyzed using an ultraviolet-visible transmission reflectometer instrument (WFH-201BJ) at 300 nm. pBR322 DNA was used as the DNA solution in all agarose gel electrophoresis experiments.

3. Results and discussion

3.1 Binding of Tb^{3+} to proteins and aggregation

3.1.1 Tb^{3+} binding to proteins. As calcium ion sensors, centrins participate in a series of cellular processes to perform their biological functions under the mode of transporting calcium ions.[27] HsCen2 belongs to the typical calcium-binding protein. As Tb^{3+} has a similar coordination chemistry and ionic radius with calcium ions, we usually use Tb^{3+} as a fluorescent probe to study the interaction between the metal ions and centrins.[28]

Based on the energy transfer from the aromatic residues on the protein to the bound Tb^{3+}, the characteristic peaks of Tb^{3+} at 490, 545, 585, and 620 nm were measured. The fluorescence spectra of Tb^{3+} in different solutions are shown in Fig. 2A. Curve a is the blank control (Hepes); curve b is free Tb^{3+} in Hepes, which can emit four characteristic peaks at 490, 545, 585, and 620 nm; curve c is Tb^{3+} in 1 mM EDTA solution; and curve d is the Tb^{3+}-sensitized fluorescence of Tb^{3+}-saturated HsCen2, after the addition of 2 Tb^{3+} to the HsCen2 solution, the fluorescence

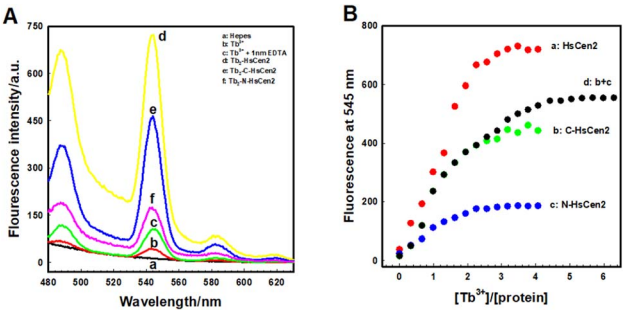

Fig. 2 (A) Fluorescence spectra of Tb^{3+}. (a) 10 mM Hepes buffer, (b) Tb^{3+} (20 μM) in 10 mM Hepes, (c) Tb^{3+} (20 μM) in 10 mM Hepes and 1 mM EDTA solution, Tb_2-HsCen2 (10 μM) (d) or Tb_2-C-HsCen2 (10 μM) (e) or Tb_2-C-HsCen2 (10 μM) (f) in 10 mM Hepes. $\lambda_{ex} = 295$ nm and 360 nm light filter was used under the present conditions. (B) Titration curves of fluorescence intensity for HsCen2 (a), C-HsCen2 (b), and N-HsCen2 (c) at 545 nm against $[Tb^{3+}]$/[protein] in 10 mM Hepes at pH 7.4.

intensity of the four characteristic peaks of Tb^{3+} increases and the average binding constant is $K_{HsCen2/Tb^{3+}} = (1.10 \pm 0.04) \times 10^5$ M^{-1}.[23] Similar phenomena of fluorescence intensity enhancement can be observed after adding Tb^{3+} to C-HsCen2 (curve e) or N-HsCen2 (curve f). The titration curves are obtained by plotting the Tb^{3+}-sensitized fluorescence intensity at 545 nm against $[Tb^{3+}]$/[protein] (Fig. 2B). It can be seen from Fig. 2B that the binding ratio of Tb^{3+} to HsCen2 (curve a) or C-HsCen2(curve b) is 2/1, and the weak sensitized fluorescence intensity when Tb^{3+} is added to N-HsCen2 may be derived from phenylalanine (Phe) residues in the protein (curve c). In addition, the superposition sum of the Tb^{3+}-sensitized fluorescence intensity of C-HsCen2 and N-HsCen2 (curve d) is less than that of HsCen2 (curve a). The plots of fluorescence intensity at 545 nm of $\log[F_i - F_0]/[F_\infty - F_i]$ against $\log[Tb^{3+}]_f$ are shown in Fig. S2. According to the method reported in the literature, it can be assumed that the two binding sites are independent and identical in proteins,[28] and the average binding constants of Tb^{3+} to C-HsCen2 and N-HsCen2 were obtained as $K_{C\text{-}HsCen2/Tb^{3+}}$, $(8.33 \pm 0.37) \times 10^4$ M^{-1} and $K_{N\text{-}HsCen2/Tb^{3+}}$, $(7.38 \pm 0.29) \times 10^2$ M^{-1} (Table 1), respectively.

Although isolated N-HsCen2 has a weak binding capacity to Tb^{3+} (10^2 M^{-1}), intact HsCen2 exhibits only two strong Tb^{3+}-binding sites at the C-terminal, while the N-terminal appears to not bind Tb^{3+}. Furthermore, the binding affinity of Tb^{3+} to HsCen2 is slightly stronger than that of Tb^{3+} to C-HsCen2, indicating that the N-terminal domain in the full-length

Table 1 Apparent average binding constants of Tb^{3+} interaction with different proteins at 30 °C

Protein	n	K_a (error)(M^{-1})
HsCen2	2.13	$(1.10 \pm 0.04) \times 10^5$
C-HsCen2	2.01	$(8.33 \pm 0.37) \times 10^4$
N-HsCen2	1.79	$(7.38 \pm 0.29) \times 10^2$

Open Access Article. Published on 14 October 2025. Downloaded on 6/14/2026 6:45:11 PM. This article is licensed under a Creative Commons Attribution-NonCommercial 3.0 Unported Licence.

Table 2 Secondary structure parameters of HsCen2 or C-HsCen2 or N-HsCen2 in the presence or absence of Tb^{3+}

Protein	I_{208}	α-helix content increases
HsCen2	−15.68	
Tb_2-HsCen2	−18.87	20.40%
C-HsCen2	−6.44	
Tb_2-C-HsCen2	−6.88	6.83%
N-HsCen2	−7.92	
Tb_2-N-HsCen2	−8.27	4.42%

molecule is beneficial to the binding of Tb^{3+} to the C-terminal domain of HsCen2, although it does not bind metal ions.

3.1.2 Tb^{3+}-induced conformational changes of proteins. The distribution of secondary structural elements in proteins was characterized by circular dichroism (CD). The shape and amplitude of the far-UV CD spectrum of HsCen2 are typical characteristics of a protein-rich α-helix.[29] When 2 equivalents of Tb^{3+} were added to HsCen2, the change in the CD signal of Tb_2-HsCen2 (Tb^{3+}-saturated HsCen2) increased by 20.4% (Table 2 and Fig. S3A).[23] Similar phenomena of CD signal intensity enhancement can be observed after adding Tb^{3+} to C-HsCen2 (Fig. S3B) or N-HsCen2 (Fig. S3C). The CD signal of HsCen2, C-HsCen2, and N-HsCen2 by Tb^{3+}-induced showed different changes. When 2 equivalents of Tb^{3+} were added to the protein, the change in the CD signal of C-HsCen2 or N-HsCen2 increased by 6.8% and 4.4% (Table 2), respectively. The results show that the conformational change of intact HsCen2 induced by Tb^{3+} binding is the most obvious change. From the amino acid sequence analysis of the protein, the sum of the lengths of isolated C-HsCen2 (1–100) and N-HsCen2 (82–172) is greater than that of intact HsCen2 (1–172). However, it can be seen from Fig. 3 that the sum of the α-helix content in C-HsCen2 and N-HsCen2 is significantly smaller than that in intact HsCen2, indicating that the C-terminal and N-terminal domains are more stable in full-length HsCen2.

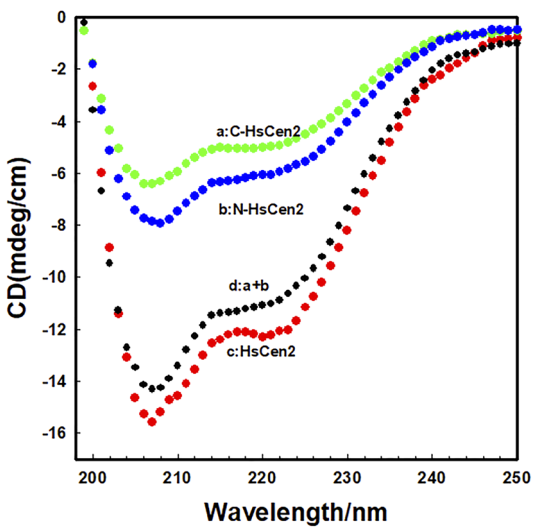

Fig. 3 Far-UV CD spectra of C-HsCen2 (curve a) or N-HsCen2 (curve b) or HsCen2 (curve c) or the calculated sum CD signals of N-HsCen2 and C-HsCen2 (curve d) using 1 mm path length quartz cells in 10 mM Hepes, pH 7.4 at 25 °C.

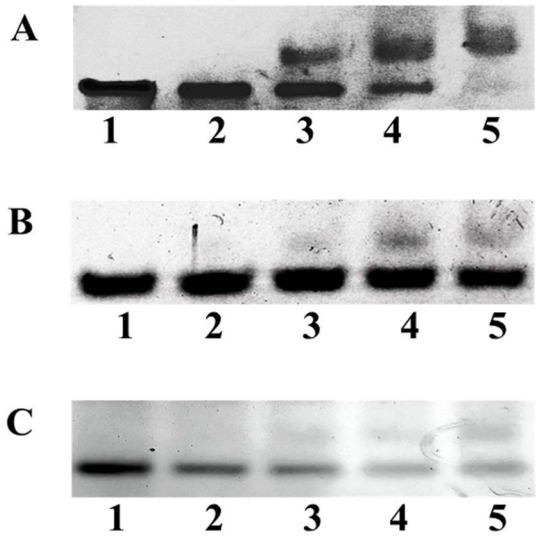

Fig. 4 Concentration gradients of the aggregation of HsCen2 (A) or C-HsCen2 (B) or N-HsCen2 (C) induced by Tb^{3+}, respectively, as monitored by 15% native-PAGE. The concentration of proteins is 120 μM. The ratio of Tb^{3+} to protein is 0.0 (1), 0.5 (2), 1.0 (3), 1.5 (4), and 2.0 (5).

3.1.3 Metal ion-induced aggregation of proteins. First, the aggregation behaviour of HsCen2, isolated C-HsCen2 and N-HsCen2 induced by Tb^{3+} was investigated by conducting native-PAGE experiments. As can be seen from Fig. 4A, there is a band of HsCen2 in lane 1, and with the increase in Tb^{3+} concentration, the band of HsCen2 is gradually decreased, and the band of Tb_2-HsCen2 is gradually increased (lane 2–5). When 2 equivalents of Tb^{3+} were added to HsCen2 solutions (lane 5), the band of HsCen2 was completely converted to the band of Tb_2-HsCen2. It is suggested that Tb^{3+} binding could induce the aggregation of HsCen2. In addition, the aggregation of C-HsCen2 (Fig. 4B) and N-HsCen2 (Fig. 4C) can also be formed. As shown in Fig. 4B and C, for both C-HsCen2 and N-HsCen2,

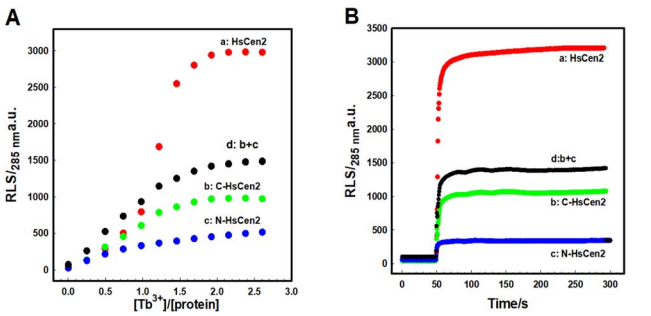

Fig. 5 (A) Titrating curves of Resonance light scattering (RLS) intensity for HsCen2 (a) or C-HsCen2 (b) or N-HsCen2 (c) at 285 nm against [Tb^{3+}]/[protein], (d) the simple sum of (b) and (c). (B) Kinetic traces followed by RLS intensity at 285 nm of HsCen2 (a), C-HsCen2 (b) or N-HsCen2 (c) with Tb^{3+}, (d) the simple sum of (b) and (c). All the experiments were conducted in 10 mM Hepes (pH 7.4) at room temperature.

© 2025 The Author(s). Published by the Royal Society of Chemistry

Open Access Article. Published on 14 October 2025. Downloaded on 6/14/2026 6:45:11 PM. This article is licensed under a Creative Commons Attribution-NonCommercial 3.0 Unported Licence.

a small number of aggregations appeared with the increase in Tb^{3+} concentration (lane 2–5). The results showed that the aggregation ability of C-HsCen2 or N-HsCen2 induced by Tb^{3+} is significantly weaker than that of HsCen2.

RLS is a valuable technique to detect the degree of aggregation of proteins in solution utilizing spectroscopy.[5] Both high protein concentration and metal ion binding contribute to protein aggregation.[14] HsCen2 can bind to two Tb^{3+}, and the binding of Tb^{3+} can cause the aggregation of HsCen2.[12] The RLS signal of C-HsCen2 and N-HsCen2 continues to increase with the increase in Tb^{3+} concentration. The titration curves of the RLS intensity of protein at 285 nm against [Tb^{3+}]/[protein] are shown in Fig. 5A. Comparison of the titration curves (Fig. 5A) of Tb^{3+} binding with proteins of HsCen2 or C-HsCen2 or N-HsCen2 suggested that Tb^{3+} binding with HsCen2 resulted in a dramatic increase in RLS signals while binding with C-HsCen2 or N-HsCen2 showed a slight increase in RLS signals. In addition, the sum of the RLS signals of C-HsCen2 and N-HsCen2 induced by Tb^{3+} (d) is significantly lower than that of HsCen2. The kinetic profile of HsCen2 (a) or C-HsCen2 (b) or N-HsCen2 (c) self-assembly induced by Tb^{3+} in 10 mM Hepes (pH 7.4) at room temperature showed an immediately exponential phase and a final stationary phase profile, without any lag phase (Fig. 5B). It can be seen intuitively from the figure that the aggregation ability of HsCen2 is obviously stronger than that of C-HsCen2 and N-HsCen2. It is shown that the aggregation of HsCen2 induced by Tb^{3+} is co-determined by both N-terminal and C-terminal domains. The molecular interactions of protein to protein are mediated probably by electrostatic and hydrophobic forces.[7] Since N-HsCen2 has a large number of positive charges and C-HsCen2 has negative charges, the aggregation of HsCen2 is mainly driven by the electrostatic interaction of the N-terminal and C-terminal domains.

3.2 Binding of protein to DNA and its endonuclease-like activity

3.2.1 DNA binding to proteins. The analysis of the binding property of DNA to HsCen2 is useful to understand the functions of centrins. The ITC thermogram of HsCen2 (80 μM) is shown in Fig. 6A, which is produced by the titration of the DNA solution (5 mM) in Hepes buffer at 30 °C. As shown in Fig. 6A, fitting the data of interaction between DNA and HsCen2 with one set of site-binding models gives affinity values, $K_{HsCen2/DNA}$, $(7.78 \pm 0.03) \times 10^3\ M^{-1}$. The thermodynamic parameters are presented in Table 3. The enthalpy change and entropy change are both positive, indicating that the binding of DNA to HsCen2 is thus mainly driven by the entropy change. The ITC diagram of the interaction between C-HsCen2 and DNA is illustrated in Fig. 6B. For DNA binding to C-HsCen2, the binding constant ($K_{C\text{-}HsCen2/DNA}$, $(1.27 \pm 0.28) \times 10^4\ M^{-1}$) is slightly larger than that of DNA binding to HsCen2. However, unlike HsCen2, the binding of DNA to C-HsCen2 is primarily driven by enthalpy changes. Similarly, DNA can bind N-HsCen2 ($K_{N\text{-}HsCen2/DNA}$, $(1.25 \pm 0.17) \times 10^3\ M^{-1}$) (Fig. 6C). The binding process is still enthalpy controlled. Detailed thermodynamic parameters are also listed in Table 3. It can be seen that the binding ability of DNA to C-HsCen2 is stronger than that of DNA to HsCen2 or N-HsCen2.

To further investigate the binding properties of protein to DNA, the fluorescence spectroscopy of protein was monitored. HsCen2 and DNA can form a 1 : 1 complex with a binding constant of $K_{HsCen2/DNA}$, $(6.30 \pm 0.01) \times 10^3\ M^{-1}$.[23] The maximum emission wavelength of C-HsCen2 is 306 nm (λ_{ex} = 295 nm) in Hepes, as plotted in Fig. 7A. With the addition of DNA into C-HsCen2, the fluorescence peak of C-HsCen2 is quenched gradually. The inset of Fig. 7A shows the titration curve obtained from the plot of fluorescence intensity of C-HsCen2 at 306 nm against [DNA]/[C-HsCen2]. With the addition of DNA, the titration curve of C-HsCen2 gradually flattens out when [DNA]/[C-HsCen2] = 1. It means that C-HsCen2 and DNA form a complex, and one molecule of C-HsCen2 can bind to one DNA. The plot of $\log[F_i - F_0]/[F_\infty - F_i]$ at 306 nm against $\log[DNA]_f$ is shown in Fig. S4, according to the literature,[37] and the binding constants of the C-HsCen2 binding to DNA can be obtained as $K_{C\text{-}HsCen2/DNA}$, $(1.18 \pm 0.23) \times 10^4\ M^{-1}$. The ability of DNA to bind to HsCen2 is weaker than that of DNA to bind to C-HsCen2. It is consistent with the results obtained by ITC (Table 3).

Fig. 7B shows the molecular docking simulation of the interaction between C-HsCen2 and DNA, where the phosphate backbone of DNA is bound within a deep cavity between the EF-3 and EF-4 domains. Since the isolated N-HsCen2 does not have luminescent amino acids, fluorescence spectroscopy cannot detect the binding of DNA to N-HsCen2. Therefore, molecular docking was used to simulate the interaction between N-HsCen2 and DNA. Fig. 7C shows that the A-helix of N-HsCen2 is inserted into the groove of DNA and can interact with DNA to form a complex. The combination mode is different from that of both C-HsCen2 and HsCen2. Since the binding ability of DNA to C-HsCen2 is greater than that of DNA to N-HsCen2, and there is a certain steric hindrance effect, only one DNA can bind to HsCen2 at C-terminal domains although C-HsCen2 and N-HsCen2 can bind DNA, respectively.

3.2.2 Conformational changes of DNA. To investigate the interactions and any structural perturbation of the DNA with HsCen2, CD spectroscopy was performed. It can be seen from Fig. 8 (black line) that DNA in buffer displays a negative CD signal at 244 nm and a positive CD signal at 277 nm, which is the characteristic peak of a typical B-type DNA structure.[30] After adding HsCen2 (red line) or C-HsCen2 (green line) or N-HsCen2 (blue line) into the DNA solution, the CD signal showed different degrees of enhancement, suggesting that the double helix structure changes a lot associated with the protein-DNA complex formation.[25] In addition, the conformational change of DNA induced by HsCen2 is significantly stronger than that of isolated C-HsCen2 and N-HsCen2. In addition, the theoretical sum of the changes in DNA conformation of isolated C-HsCen2 and N-HsCen2 (brown line) is significantly larger than that of intact HsCen2. The results showed that the C-terminal and N-terminal domains of HsCen2 may have a certain cooperative effect on the change in DNA conformation.

3.2.3 Endonuclease-like activity of proteins. DNA binding to protein is a critical step for subsequent cleavage. The agarose

Open Access Article. Published on 14 October 2025. Downloaded on 6/14/2026 6:45:11 PM.
This article is licensed under a Creative Commons Attribution-NonCommercial 3.0 Unported Licence.

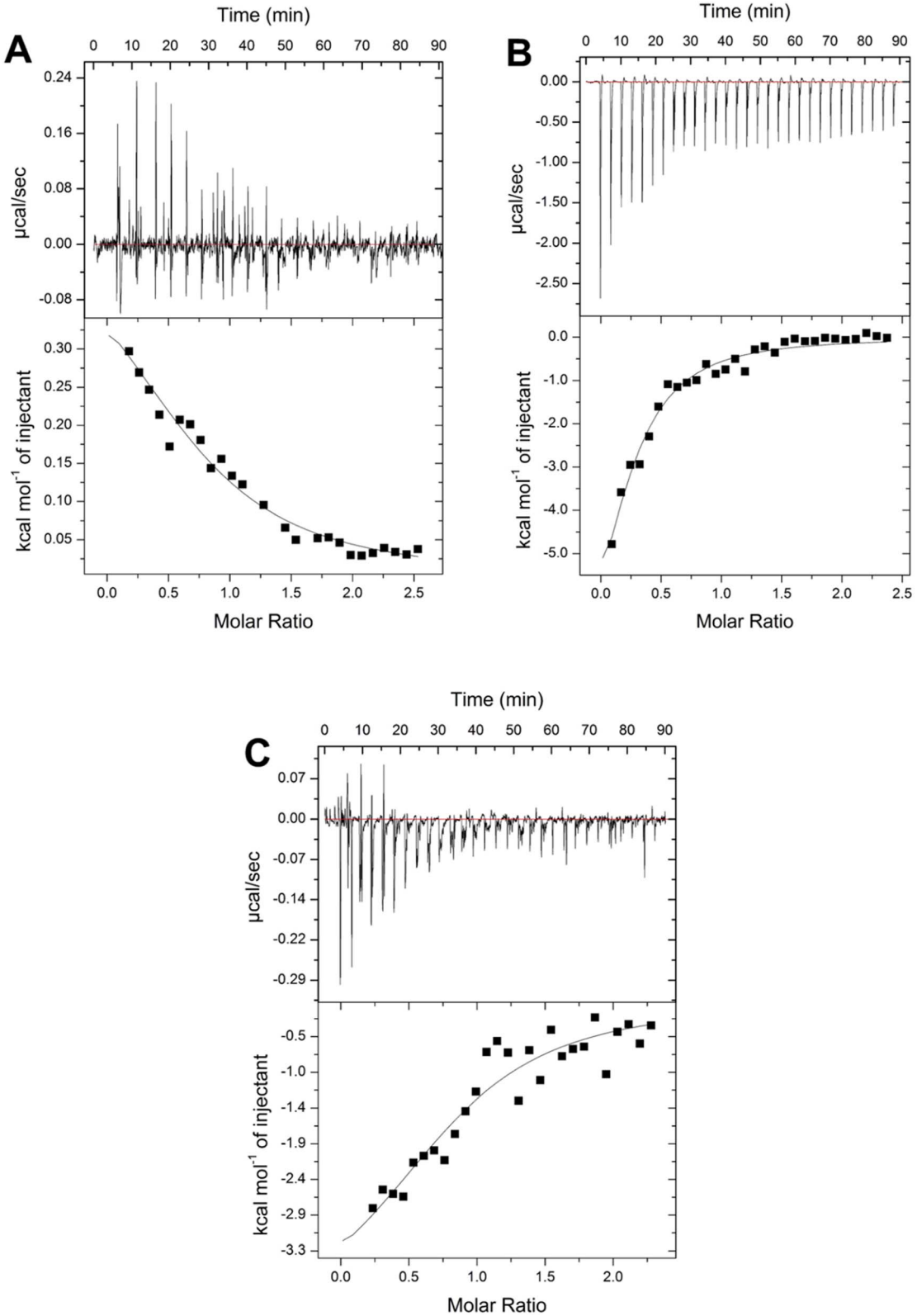

Fig. 6 Thermograms (top panels) and isotherms (bottom panels) of the titration of DNA (5 mM) into 80 μM HsCen2 (A) or C-HsCen2 (B) or N-HsCen2 (C) at 30 °C.

gel electrophoresis results of pBR322 DNA (0.005 μg μL^{-1}) cleavage after incubation with different proteins (10 μM) for 3 h at 4 °C are shown in Fig. 9. It is found that pBR322 DNA can be cleaved by HsCen2, isolated C-HsCen2, and isolated N-HsCen2. The supercoiled DNA (Form I, lower band in lane 1) breakage results in the formation of nicked circular DNA (Form II, upper

© 2025 The Author(s). Published by the Royal Society of Chemistry

Open Access Article. Published on 14 October 2025. Downloaded on 6/14/2026 6:45:11 PM. This article is licensed under a Creative Commons Attribution-NonCommercial 3.0 Unported Licence.

Table 3 Thermodynamic parameters of DNA interaction with different proteins at 30 °C

Protein	n	$K_a/(M^{-1})$	$\Delta G/(kcal\ mol^{-1})^a$	$\Delta H/(kcal\ mol^{-1})^a$	$\Delta S/(cal\ mol^{-1}\ deg^{-1})^a$
HsCen2	0.77^a	$(7.78 \pm 0.03) \times 10^{3a}$	−5.26	0.50 ± 0.06	19.00
	0.85^b	$(6.30 \pm 0.01) \times 10^{3b}$			
C-HsCen2	1.00^a	$(1.27 \pm 0.28) \times 10^{4a}$	−5.61	−10.29 ± 0.26	−15.20
	0.82^b	$(1.18 \pm 0.23) \times 10^{4b}$			
N-HsCen2	0.98^a	$(1.25 \pm 0.17) \times 10^{3a}$	−4.27	−6.03 ± 0.50	−5.71

[a] Data from ITC titrations. [b] Data from spectrofluorimetric titrations.

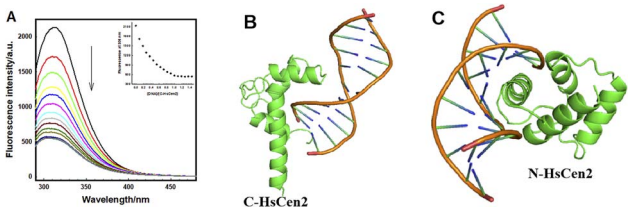

Fig. 7 (A) Fluorescence spectra of C-HsCen2 with the addition of DNA in 10 mM Hepes at pH 7.4. Inset: the plot of fluorescence intensity for C-HsCen2 at 306 nm against [DNA]/[protein]. Schematic representation of C-HsCen2 (PDB:2GGM) (B) and N-HsCen2 (C) interaction with DNA (PDB:1DJD) by ZDOCK 3.0.2.

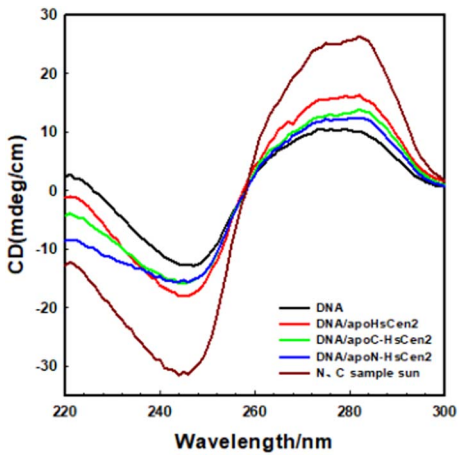

Fig. 8 Far-UV CD spectra of DNA interaction with HsCen2 or C-HsCen2 or N-HsCen2 in 10 mM Hepes, pH 7.4, [protein] = 5 μM, [DNA] = 5 μM.

band in lane 2) in the presence of HsCen2. Linear DNA (Form III, middle band) appears in the presence of C-HsCen2 (lane 3) or N-HsCen2 (lane 4). HsCen2 has certain endonuclease-like activity, and the endonuclease-like activity of C-HsCen2 or N-HsCen2 is much higher than that of HsCen2 under the same conditions. Comparing lane 3 and lane 4, it can be seen that the content of Form II DNA in lane 4 is more than that in lane 3, indicating that the endonuclease-like activity of N-HsCen2 is stronger than that of C-HsCen2.

pBR322 DNA (0.005 μg μL^{-1}) was completely cleavage into notched and linear DNA by HsCen2 (1000 μM) and incubated for 5 h at 4 °C.[29] On this basis, the cleavage of supercoiled DNA by half-molecules was investigated. Fig. 10 presents the agarose gel electrophoresis results for the cleavage of pBR322 DNA after incubation with C-HsCen2 (Fig. 10A) or N-HsCen2 (Fig. 10B) at different concentrations. When proteins are not added, the supercoiled DNA is a complete band (lane 1); upon the addition of proteins, supercoiled DNA is cleaved into nicked circular and linear DNA; when the supercoiled DNA disappears and is completely cleaved into nicked circular and linear DNA, the required protein concentrations of C-HsCen2 or N-HsCen2 are 105 μM and 26 μM, respectively. It shows that the N-HsCen2 has the highest endonuclease-like activity. The plots of contents of Form I, Form II and Form III DNA against the concentration of C-HsCen2 (Fig. S5A) and N-HsCen2 (Fig. S5B) are shown in Fig. S5. It can be clearly seen from the figure that as the protein concentration increases, the content of Form I DNA gradually decreases, while the contents of Form II and Form III DNA gradually increase.

The agarose gel electrophoresis results of C-HsCen2 (105 μM) or N-HsCen2 (26 μM) and pBR322 DNA (0.005 μg μL^{-1}) incubation at different times are shown in Fig. 11. With the increase in incubation time, Form I of the supercoiled DNA was cleaved into Form II DNA, immediately after which the structure of Form II DNA was gradually transformed into Form III linear DNA. HsCen2 (1000 μM) can completely cleave supercoiled DNA within 5 h.[23] As can be seen from Fig. 11A and B, C-HsCen2 (105 μM) or N-HsCen2 (26 μM) required 5.5 h and 2.25 h to completely cleave supercoiled DNA, respectively. Taking the Form I supercoiled DNA cleavage as a marker, the plots of contents of Form I supercoiled DNA against the time are shown in Fig. S6. The contents of Form I supercoiled DNA plots against time are fitted with the aid of a single exponential fitting program. For the convenience of comparison, the rate constant is converted into a molar rate constant. k_IM of HsCen2 or C-HsCen2 or N-HsCen2 cleavage supercoiled DNA is (0.62 ±

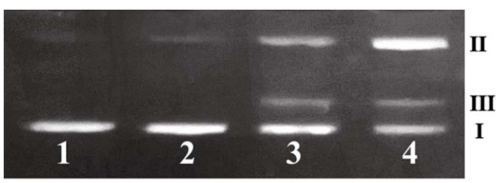

Fig. 9 Agarose gel electrophoresis of pBR322 DNA (0.005 μg μL^{-1}) cleavage after incubation with HsCen2 or C-HsCen2 or N-HsCen2 (10 μM) for 3 h at 4 °C, lane 1: control untreated supercoiled DNA, lane 2: DNA + HsCen2, lane 3: DNA + C-HsCen2, lane 4: DNA + N-HsCen2.

Open Access Article. Published on 14 October 2025. Downloaded on 6/14/2026 6:45:11 PM. This article is licensed under a Creative Commons Attribution-NonCommercial 3.0 Unported Licence.

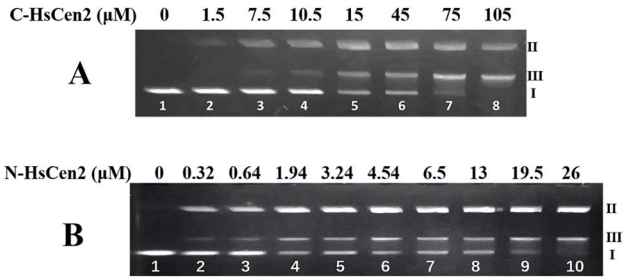

Fig. 10 Agarose gel electrophoresis of pBR322 DNA (0.005 μg μL^{-1}) after incubation with C-HsCen2 (A) or N-HsCen2 (B) at different concentrations for 5 h at 4 °C.

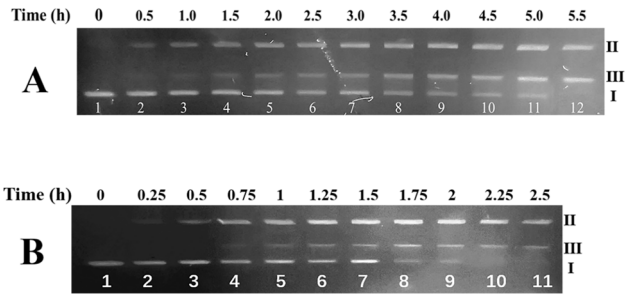

Fig. 11 Agarose gel electrophoresis of pBR322 DNA (0.005 μg μL^{-1}) after incubation with C-HsCen2 (A, 105 μM) or N-HsCen2 (B, 26 μM) for different time, respectively.

0.06), (3.62 ± 0.67), and (33.85 ± 3.08) × 10^3 h^{-1} M^{-1}, respectively (Table 4). This further supports the order of endonuclease-like activity: N-HsCen2 > C-HsCen2 > HsCen2.

The hydroxyl group of Ser and Thr performs a nucleophilic attack on the phosphorus center of DNA, resulting in the formation of a pentacoordinate phosphorus transition state and efficient DNA cleavage.[33] It is speculated that the binding mode of the N-terminal to DNA facilitates the approach of Ser and Thr to the phosphorus center, thereby promoting hydrolysis and exhibiting strong endonuclease-like activity.

3.3 Cooperative effect between the N- and C-terminal domains of HsCen2

3.3.1 GdnHCl-induced unfolding of HsCen2. The mechanism by which proteins fold to their unique native conformations from an initially disorganized form is one of the fundamental problems in molecular biology.[31] The primary structure of a protein usually contains one or more inactive peptide chains that need to be folded into specific stereoscopic structures to perform their functions. The study of protein folding and unfolding is of great significance in understanding its structure and function.[32] Denaturants denature proteins by reducing their stability and changing their structure from a specific, compact three-dimensional structure to a fully unfolded state. Guanidine hydrochloride (GdnHCl) is a commonly used denaturant. The thermodynamic stability of proteins can be measured by the protein unfolding induced by GdnHCl.[31]

The CD spectrum of HsCen2 has two characteristic peaks at 208 and 222 nm in a natural state (curve a in Fig. 12A). The characteristic peak of HsCen2 at 222 nm gradually decreased with the increase in GdnHCl concentration (curve b–e), indicating that the higher order structure of HsCen2 is unfolded in the GdnHCl solution. The curves for GdnHCl-induced unfolding of HsCen2 (curve a) or C-HsCen2 (curve b) or N-HsCen2 (curve c) at 222 nm are shown in Fig. 12B. It can be seen that at lower GdnHCl concentrations, the percentage of unfolding is 0, and the protein is completely in the folded state. The percentage of unfolding increases with the increase in GdnHCl concentration. When the GdnHCl concentration reaches a certain value, the percentage of unfolding reaches 1, indicating that the protein has been completely unfolded. It shows that the unfolding curves of C-HsCen2 (curve b in Fig. 12B) and N-HsCen2 (curve c in Fig. 12B) caused by GdnHCl are a typical two-state transition model ($N \rightleftharpoons U$). The corresponding thermodynamic parameters are listed in Table 5. As can be seen from the data, the unfolding of C-HsCen2 and N-HsCen2 is induced by GdnHCl, with $\Delta G^0(H_2O)$ of 1.38 and 5.70 kcal mol^{-1}, respectively. It shows that the stability of N-HsCen2 is greater than that of C-HsCen2.

The unfolding of HsCen2 (curve a in Fig. 12B) appears to involve two sequential transitions (curve a1 and a2 in Fig. S7A), which indicate that the equilibrium unfolding reactions are three-state reactions ($N \rightleftharpoons I \rightleftharpoons U$). It can be seen that there is a small plateau between 1.2 and 2 M of GdnHCl, indicating that there is partial unfolding in this GdnHCl concentration range. According to the model proposed by our group,[33,34] the two transitions can be attributed to two structural elements existing in HsCen2. The first structural element was considered to be the

Table 4 Kinetic parameters of DNA hydrolysis catalyzed by different proteins

Protein	k_l(h^{-1})	K_I^M (error) (10^3 h^{-1} M^{-1})
HsCen2 (1000 μM)	0.62 ± 0.06	0.62 ± 0.06
C-HsCen2 (105 μM)	0.38 ± 0.03	3.62 ± 0.67
N-HsCen2 (26 μM)	0.88 ± 0.10	33.85 ± 3.08

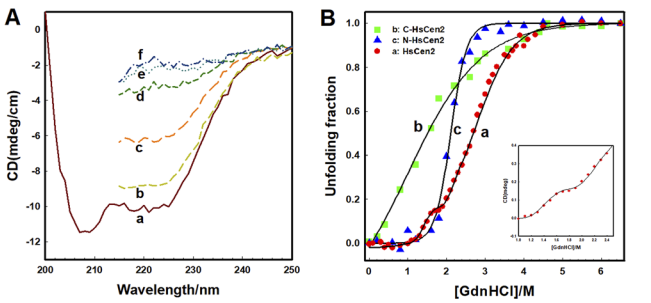

Fig. 12 (A) Far-UV CD spectra of HsCen2 (a) and HsCen2 at different concentrations of GdnHCl (b–f). (B) Curves of GdnHCl-induced unfolding of HsCen2 (a) or C-HsCen2 (b) or N-HsCen2 (c) in 10 mM Hepes, pH 7.4, at 25 °C. Inset: magnified view of the corresponding HsCen2 unfolding curve (1.0–2.5 M GdnHCl).

© 2025 The Author(s). Published by the Royal Society of Chemistry

Open Access Article. Published on 14 October 2025. Downloaded on 6/14/2026 6:45:11 PM. This article is licensed under a Creative Commons Attribution-NonCommercial 3.0 Unported Licence.

Table 5 Thermodynamic parameters of different proteins from GdnHCl-induced unfolding at pH 7.4, 25 °C

Protein	Parameters	$F \leftrightarrow I/U$	$I \leftrightarrow U$	$\langle\Delta G^0_{element}\rangle$ (kcal mol^{-1})
HsCen2	$[D]_{1/2}$(mol)	1.48 ± 0.02	2.81 ± 0.03	4.14
	-m(kcal L mol^{-2})	4.83 ± 0.08	1.28 ± 0.03	
	ΔG^0_I(kcal mol^{-1})	7.16 ± 0.08	3.80 ± 0.07	
C-HsCen2	$[D]_{1/2}$(mol)	1.58 ± 0.37		
	-m(kcal L mol^{-2})	0.87 ± 0.02		
	ΔG^0_C(kcal mol^{-1})	1.38 ± 0.05		
N-HsCen2	$[D]_{1/2}$(mol)	2.10 ± 0.01		
	-m(kcal L mol^{-2})	2.65 ± 0.06		
	ΔG^0_N(kcal mol^{-1})	5.70 ± 0.11		

C-terminal (curve a1 in Fig. S7A), and the second structural element was identified as the N-terminal (curve a2 in Fig. S7A).[35] $\Delta G^0(H_2O)$ of the first structural element ($N \rightleftharpoons I$) and second structural element ($I \rightleftharpoons U$) for HsCen2 is 7.16 and 3.80 kcal mol^{-1} (Fig. S7B), respectively. The data in Table 5 show that the C-terminal domain of HsCen2 is more sensitive to denaturants compared with isolated C-HsCen2, and its relative stability is enhanced. However, the N-terminal domain of HsCen2 is less sensitive to denaturants than the isolated N-HsCen2, and the relative stability of the N-terminal domain of HsCen2 is weakened. $\Delta G^0(H_2O)$ of HsCen2 is 10.96 kcal mol^{-1}, while the sum of $\Delta G^0_C(H_2O)$ and $\Delta G^0_N(H_2O)$ for C-HsCen2 and N-HsCen2 is 7.08 kcal mol^{-1}. It means that the stability of HsCen2 is greater than that of C-HsCen2 or N-HsCen2.

3.3.2. Cooperative effect. Protein folding is a highly cooperative process. In most situations, the folding–unfolding equilibrium is well accounted for by a two-state process in which the population of intermediates is assumed to be zero.[36] Despite this fact, there is ample evidence, indicating that certain residues become exposed to the solvent as a result of local rather than global unfolding.[33] From a rigorous point of view, cooperativity originates when the partition function of a system cannot be written as the sum of the individual partition functions of the constituent subsystems.[37]

The GdnHCl-induced unfolding experiment showed that the stability of the C-terminal domain of HsCen2($\Delta G^0(H_2O)$ = 7.16 kcal mol^{-1}) is greater than that of isolated C-HsCen2($\Delta G^0(H_2O)$ = 1.38 kcal mol^{-1}), while the stability of N-terminal domain of HsCen2($\Delta G^0(H_2O)$ = 3.80 kcal mol^{-1}) is lower than that of isolated N-HsCen2($\Delta G^0(H_2O)$ = 5.70 kcal mol^{-1}). Moreover, the unfolding free energy of HsCen2 induced by GdnHCl is not equal to the sum of the unfolding free energies of C-HsCen2 and N-HsCen2. In the presence of the N-terminal domain of HsCen2, the C-terminal domain of HsCen2 is more sensitive to denaturants and its stability is enhanced, and in the presence of the C-terminal domain of HsCen2, the N-terminal domain of HsCen2 is less sensitive to denaturants and its stability is decreased. It is proved that there are cooperative effects between the N-terminal and C-terminal domains of HsCen2. It is the cooperative effects that make HsCen2 bind only 2 Tb^{3+} at C-terminal domains although C-HsCen2 and N-HsCen2 can bind 2 Tb^{3+}, respectively. Despite both isolated C-HsCen2 and N-HsCen2 being capable of DNA binding, a cooperative effects within the full-length HsCen2 ensures that DNA binding occurs exclusively at the C-terminal domain. Although N-HsCen2 has the highest endonuclease-like activity, the cooperative effects make the endonuclease-like activity of HsCen2 lowest.

4. Conclusions

In this work, we investigated some properties and functions of HsCen2, isolated C-HsCen2, and isolated N-HsCen2 using a variety of biological and chemical methods. The Tb^{3+} binding data demonstrate that the N-terminal domain promotes Tb^{3+} binding at the C-terminal domain of HsCen2. Metal ion binding can induce the formation of protein aggregates, and the aggregation of HsCen2 induced by metal ions is co-determined by both the N-terminal domain and C-terminal domains. In addition, in the binding of proteins to DNA, we found that the binding ability of the isolated C-terminal domain to DNA is greater than that of intact HsCen2 to DNA. After binding to DNA, centrin exhibits a certain endonuclease-like activity and can hydrolyse DNA. In addition, N-HsCen2 has the highest endonuclease-like activity compared to that of C-HsCen2 and HsCen2. Extensive experimental results show that the intact HsCen2 molecules differ from the isolated N- and C-terminal domains in multiple properties and functions. There exists a cooperative effect in HsCen2 between the N- and C-terminal domains.

Conflicts of interest

There are no conflicts to declare.

Data availability

Data supporting this study are available in the article or its supplementary information (SI).

Supplementary information is available. See DOI: **https://doi.org/10.1039/d5ra04219d**.

Acknowledgements

This work was supported by the National Natural Science Foundation of PR China [No. 21571117, No. 20901048, and No. 20771068], the Natural Science Foundation of Shanxi Province [No. 201801D121198 and No. 202103021224021], the

Open Access Article. Published on 14 October 2025. Downloaded on 6/14/2026 6:45:11 PM. This article is licensed under a Creative Commons Attribution-NonCommercial 3.0 Unported Licence.

Department of Education Fund Project of Shanxi Province [No. 2025L136], Scientific Research Initiation Fund Project of Taiyuan University [No. 25TYKY121] and the Scientific Research Project of Taiyuan University [No. 23TYQN21].

Notes and references

1 R. Errabolu, M. A. Sanders and J. L. Salisbury, *J. Cell Sci.*, 1994, **107**, 9–16.
2 J. L. Gifford, M. P. Walsh and H. J. Vogel, *Biochem. J.*, 2007, **405**, 199–221.
3 E. Matei, S. Miron, Y. Blouquit, P. Duchambon, I. Durussel, J. A. Cox and C. T. Craescu, *Biochemistry*, 2003, **42**, 1439–1450.
4 S. Veeraraghavan, P. A. Fagan, H. Hu, V. Lee, J. F. Harper, B. Huang and W. J. Chazin, *J. Biol. Chem.*, 2002, **277**, 28564–28571.
5 Y. Q. Zhao, X. J. Guo and B. S. Yang, *Int. J. Biol. Macromol.*, 2019, **128**, 314–323.
6 M. Pedretti, L. Bombardi, C. Conter, F. Favretto, P. Dominici and A. Astegno, *Int. J. Mol. Sci.*, 2021, **22**, 12173.
7 A. Yang, S. Miron, P. Duchambon and L. Assairi, *Biochemistry*, 2006, **45**, 880–889.
8 B. Pastrana-Rios, *J. Mol. Struct.*, 2014, **1069**, 85–88.
9 J. A. Cox, F. Tirone, I. Durussel, C. Firanescu, Y. Blouquit, P. Duchambon and C. T. Craescu, *Biochemistry*, 2005, **44**, 840–850.
10 Y. Q. Zhao, J. Yang, J. B. Chao and B. S. Yang, *Int. J. Biol. Macromol.*, 2019, **136**, 503–511.
11 A. Popescu, S. Miron, Y. Blouquit, P. Duchambon, P. Christova and C. T. Craescu, *J. Biol. Chem.*, 2003, **278**, 40252–402561.
12 M. Tourbez, C. Firanescu, A. Yang, L. Unipan, P. Duchambon, Y. Blouquit and C. T. Craescu, *J. Biol. Chem.*, 2004, **279**, 47672–47680.
13 Y. Q. Zhao, X. J. Guo and B. S. Yang, *RSC Adv.*, 2017, **7**, 10206–10214.
14 L. Duan, Y. Q. Zhao, Z. J. Wang, G. T. Li, A. H. Liang and B. S. Yang, *J. Inorg. Biochem.*, 2008, **102**, 268–277.
15 Y. Q. Zhao, L. Song, A. H. Liang and B. S. Yang, *J. Photochem. Photobiol. B*, 2009, **95**, 26–32.
16 W. L. Zhang, E. X. Shi, Y. Q. Zhao and B. S. Yang, *J. Inorg. Biochem.*, 2018, **186**, 280–293.
17 J. L. Salisbury, K. M. Suino, R. Busby and M. Springett, *Curr. Biol.*, 2002, **12**, 1287–1292.
18 A. Paoletti, M. Moudjou, M. Paintrand, J. L. Salisbury and M. Bornens, *J. Cell Sci.*, 1996, **109**, 3089–3102.
19 M. Araki, C. Masutani, M. Takemura, A. Uchida, K. Sugasawa, J. Kondoh, Y. Ohkuma and F. Hanaoka, *J. Biol. Chem.*, 2001, **276**, 18665–18672.
20 R. Nishi, Y. Okuda, E. Watanabe, T. Mori, S. Iwai, C. Masutani, K. Sugasawa and F. Hanaoka, *Mol. Cell. Biol.*, 2005, **25**, 5664–5674.
21 R. Nishi, W. Sakai, D. Tone, F. Hanaoka and K. Sugasawa, *Nucleic Acids Res.*, 2013, **41**, 6917–6929.
22 Y. S. Krasikova, N. I. Rechkunova, E. A. Maltseva, C. T. Craescu, I. O. Petruseva and O. I. Lavrik, *Biochemistry*, 2012, **77**, 346–353.
23 J. Yang, Y. Q. Zhao and B. S. Yang, *RSC Adv.*, 2022, **12**, 21892.
24 Y. Q. Zhao, X. F. Cui, J. Yang, L. Yu and B. S. Yang, *Electrochim. Acta*, 2019, **298**, 518–524.
25 W. L. Zhang, E. X. Shi, Y. Feng, Y. Q. Zhao and B. S. Yang, *RSC Adv.*, 2017, **7**, 51773–51788.
26 T. Vreven, B. G. Pierce, H. Hwang and Z. Weng, *Proteins*, 2013, **81**, 2175–2182.
27 Y. Zhang and C. Y. He, *Protoplasma*, 2012, **249**, 459–467.
28 J. Yang, Y. Q. Zhao and B. S. Yang, *RSC Adv.*, 2022, **12**, 21892–21903.
29 Y. X. Song, Z. Song and B. S. Yang, *Chem. Res. Chinese U.*, 2019, **35**, 53–59.
30 J. Kypr, I. Kejnovska, D. Renciuk and M. Vorlıckova, *Nucleic Acids Res.*, 2009, **37**, 1713–1725.
31 Z. Song, X. Y. Zheng and B. S. Yang, *Protein Sci.*, 2013, **22**, 1519–1530.
32 C. R. Matthews and M. M. Crisanti, *Biochemistry*, 1981, **20**, 784–792.
33 B. S. Yang, Z. Song, X. Y. Zheng and Y. Q. Zhao, *Sci. China Chem.*, 2012, **55**, 1351–1357.
34 B. S. Yang, J. Ming and Z. Song, *Sci. China Chem.*, 2014, **44**, 646–653.
35 Z. Song, J. Ming and B. S. Yang, *J. Biol. Inorg. Chem.*, 2014, **19**, 359–374.
36 L. Reich and T. R. Weikl, *Proteins*, 2006, **63**, 1052–1058.
37 H. Q. Li, Y. Q. Zhao and B. S. Yang, *Chin. J. Chem.*, 2009, **27**, 1762–1766.

© 2025 The Author(s). Published by the Royal Society of Chemistry